NANO LETTERS

pubs.acs.org/NanoLett

Letter

Ultrathin Tunable Optomechanical Metalens

Adeel Afridi, Jan Gieseler, Nadine Meyer, and Romain Quidant*

Cite This: *Nano Lett.* 2023, 23, 2496–2501

Read Online

ACCESS | Metrics & More | Article Recommendations | Supporting Information

ABSTRACT: Reconfigurable metasurfaces offer great promises to enhance photonics technology by combining integration with improved functionalities. Recently, reconfigurability in otherwise static metasurfaces has been achieved by modifying the electric permittivity of the meta-atoms themselves or their immediate surrounding. Yet, it remains challenging to achieve significant and fast tunability without increasing bulkiness. Here, we demonstrate an ultrathin tunable metalens whose focal distance can be changed through optomechanical control with moderate continuous wave intensities. We achieve fast focal length changes of more than 5% with response time of the order of 10 μs.

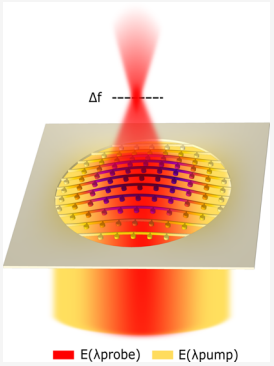

KEYWORDS: *Optomechanics, Reconfigurable metasurface, Nanophotonics, Metalens*

A metalens is a two-dimensional (2D) metasurface[1−3] that controls the amplitude, polarization, and phase of the impinging light using engineered sub-wavelength resonators, also known as meta-atoms (MA), judicially arranged in periodic or quasi-periodic arrays.[2,4−6] To date, metalenses are the center of intense research efforts and have shown great potential to replace bulky optical elements, sometimes even with superior performance.[7] However, the intrinsic passive nature of metalenses limits their use where active operation is required, such as adaptive vision and imaging.[5−12] To address this challenge, various approaches have emerged that rely on changing the optical properties of the meta-atoms themselves or their surrounding medium.[6,12−26] In particular, promising advances were reported using electro-optic control,[12,16−18] temperature-induced effects,[19,20] light-induced effects,[21−25] phase change media,[26] and mechanical actuation.[6,13−15] Despite this progress, it remains challenging to combine compactness, fast operation speed, and low energy consumption. For instance, a phase-change material-based metasurface provides large tunability and ultrafast switch ON time (up to MHz) but suffers from long switch OFF time.[27] Similarly, electrically controlled liquid crystal (LC) embedded metalenses operate at low driving voltages (<10 V). However, they require bulky LC chambers and are polarization-dependent due to the birefringence of the LC.[12,28] Microelectromechanical systems (MEMS)-based technologies promise large focal length changes and high switching speed but require high driving voltages.[6,15] On the other hand, mechanical stretching requires bulky mechanical arms limiting integration and response time.[14]

Optomechanics,[29−35] where optical forces mediate the interaction between light and structural mechanics, offers new possibilities for reconfigurable metasurfaces. When considering suspended meta-atoms patterned in a thin membrane, the enhanced electromagnetic forces at resonance can exceed elastic forces of the material, thereby inducing mechanical deformation. Already a small deformation alters the phase delay incurred by the impinging light substantially.[36] First proposed theoretically,[37] the concept of optomechanical metasurfaces features giant nonlinearity, optical bistability, and asymmetric light transmission. Shortly after, optomechanically induced modulation of light transmission through a metasurface was experimentally demonstrated.[38] Similarly, gold meta-atoms supported by pairs of free-standing silicon nitride strings exhibit individual optomechanical plasmonic resonances.[39] An experimental study of a suspended silicon carbide (SiC) metasurface supporting multimode vibrational resonances was reported.[40] More recently, an experimental demonstration of nonreciprocal transmission and optical bistability at low intensity (~10 W/cm^2) in a free-standing Si_3N_4 membrane-based metasurface was presented.[41] These observations suggest optomechanical control as a promising approach toward compact, fast, and low-power tunable metalenses.

In this Communication, we design, fabricate, and characterize an ultrathin optomechanically reconfigurable metalens operating in the near-IR regime. Our metalens is formed by an

Received: October 19, 2022
Revised: March 15, 2023
Published: March 23, 2023

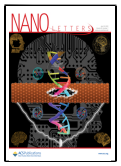

https://doi.org/10.1021/acs.nanolett.2c04105
Nano Lett. 2023, 23, 2496−2501

ensemble of suspended Huygens' meta-atoms[42] carved in a free-standing crystalline silicon membrane, as illustrated in Figure 1. The metalens is designed to focus the probe light at

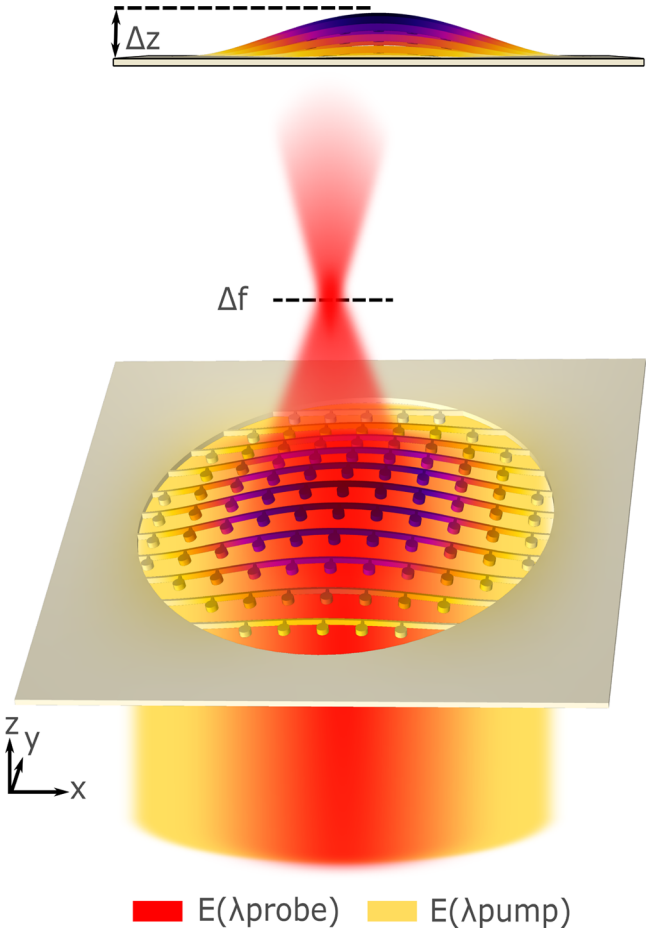

Figure 1. Artistic representation of an optomechanically reconfigurable metalens. The metalens is designed to focus light at λ_{probe}. Upon illumination with a pump beam at λ_{pump}, the resonantly enhanced optical force mechanically deforms the metalens by an amount Δz resulting in a change of the focal length (Δf) at λ_{probe}.

λ_{probe} = 1.31 μm while being controlled by a pump beam at λ_{pump} = 1.55 μm. Optical forces experienced by the meta-atoms translate into a mechanical deformation of the metalens (Δz) and consequently a change in the focal length Δf. Beyond demonstrating the tunability of the focal length by the pump light, we perform a full characterization of the lens performance including power dependence, focusing efficiency, and time response.

Combining light focusing with optomechanical control requires careful multimode engineering at both pump and probe wavelengths. On the one hand, the set of meta-atoms must cover phase changes from 0 to 2π at λ_{probe}. On the other hand, an additional mode at λ_{pump} is required to induce optical forces causing a sufficiently large mechanical deformation. To meet these requirements, we selected a rectangular periodic arrangement of suspended Huygens' meta-atoms with periodicity P_x (P_y) along the x (y) axis, in a 200 nm-thick silicon membrane. Each meta-atom consists of a disk with radius r, attached to a transversal nanobeam of width w_2 via a short neck of width w_1 (Figure 2a). Design optimization used a commercial finite element method simulator (COMSOL

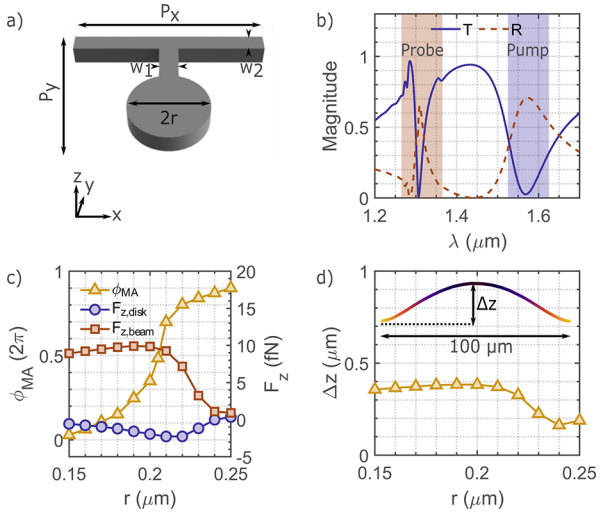

Figure 2. Geometry and simulation results of the silicon meta-atom. (a) Meta-atom geometrical parameters. (b) Simulated transmission T (blue solid line) and reflection R (red dashed line) of a meta-atom with disk radius r = 0.2 μm. The red (blue) shaded region signifies probe (pump) resonance. (c) Simulated phase due to the meta-atoms at probe wavelength λ_{probe} = 1.31 μm and calculated force experienced by the meta-atoms at pump wavelength λ_{pump} = 1.55 μm and pump intensity I_p = 1 μW/μm^2, as a function of disk radius r. (d) Numerical simulation of the deformation Δz for meta-atoms in a 1D array in the presence of pump light with I_p = 110 μW/μm^2.

MULTIPHYSICS). Figure 2b displays the transmission T and reflection R for a specific meta-atom with r = 0.2 μm, w_1 = w_2 = 0.095 μm, and P_x = P_y = 1.275 μm. Under x-polarized light, the disk supports magnetic and electric dipolar resonances around λ_{probe} = 1.31 μm. The interaction between the electric and magnetic dipole resonances, controlled by the disk radius r, introduces a phase delay of the incoming light.[42,43] Additionally, the disk attached to the supporting beam supports an electric mode around λ_{pump}, which we use for optomechanical control.

Next, we optimized an entire set of meta-atoms to provide 0−2π phase change at λ_{probe}, by changing the disk radius r and beam width w_2 simultaneously. The simulated phase imparted (ϕ_{MA}) by these meta-atoms at λ_{probe} are shown in Figure 2c as a function of r (yellow solid line with triangular markers), while the respective w_2 parameter is given in Table 1 in the Supporting Information. The periodicity and the width were kept constant at P_x = P_y = 1.275 μm and w_1 = 0.095 μm, respectively.

In addition, we used the time-averaged Maxwell's stress tensors to calculate the optical forces acting on the meta-atoms, as a function of the disc radius r (see Supporting Information for details). Figure 2c shows that the subunit (see Figure S4a in Supporting Information) of the meta-atoms experiences antiparallel forces along the z-direction, while the forces cancel out in the xy plane. The disk experiences a negative force that pulls against the illumination direction. Conversely, the beam is pushed by the incoming light. This force imbalance across the meta-atom introduces a tilt of the disk with respect to the beam, while the total positive force over a finite periodic array bends the whole array forward. Furthermore, we numerically simulated the deformation Δz, for a maximum pump intensity of I_p = 110 μW/μm^2 for each meta-atom arranged equidistantly in a one-dimensional (1D) array of 100 μm.[37] Figure 2d shows the deformation Δz as a

https://doi.org/10.1021/acs.nanolett.2c04105
Nano Lett. 2023, 23, 2496−2501

function of disk radius r. We observe a maximum deformation $\Delta z \approx 380$ nm for the meta-atom with $r = 200$ nm. Heating of the metalens under pump illumination induces thermal expansion and bending in the suspended meta-atoms. In order to quantify the thermal effects, we simulated the thermal distribution for each meta-atom using COMSOL MULTIPHYSIS (see Supporting Information for method). Figure S1b shows the temperature distribution for a meta-atom array with $r = 0.22$ μm for $I_p = 110$ μW/μm^2. Similarly, Figure S1c shows the maximum temperature change ΔT_{max} for all the meta-atoms in the library. The maximum $\Delta T_{max} = 250$ K occurs for the meta-atom with radius $r = 0.21$ μm. Based on the coefficient of thermal expansion of silicon,[44−46] the thermally induced buckling of the array of length $L = 100$ μm is expected to be of only few nanometers. From these simulations, we conclude that the thermal expansion is negligible when compared to the optomechanically induced deformation.

To calculate the required phase profile $\phi_{req}(x, y)$ in the xy-plane, which focuses light at focal length f, we used the hyperboloidal phase function.

$$\phi_{req}(x, y) = \frac{2\pi}{\lambda_{probe}}(\sqrt{x^2 + y^2 + f^2} - f)$$

We fixed the focal distance and diameter of the metalens at $f = 300$ μm and $D = 100$ μm, respectively. We discretized the continuous $\phi_{req}(x, y)$ with a suitable meta-atom such that, at a given x and y position, $|\phi_{MA} - \phi_{req}(x, y)|$ is minimized.

To fabricate our tunable metalens design, we employed top-down electron beam (E-beam) lithography. As material substrate we used a commercially available free-standing crystalline (100) silicon membrane from Norcada Inc. We spin-coated the membrane sample with the AR-P 6200.04 positive e-beam resist with a thickness of 230 nm followed by baking for 1 min at 150 °C. Afterward, E-beam exposure was carried out followed by one and a half minutes of development in an AR 600-546 developer at room temperature. We then etched the silicon membrane using HBr chemistry with an inductively coupled plasma (ICP) etcher. Finally, we stripped off the photoresist with an oxygen plasma etcher. Figure 3 shows scanning electron microscopy (SEM) images of the final metalens with a diameter $D = 100$ μm and designed focal length $f = 300$ μm.

We characterized the fabricated metalens using a homemade two-color optical setup (see Figure S2 of the Supporting Information). Collimated probe and pump beams are linearly polarized. The pump beam passes through a combination of an electro opto modulator (EOM), a polarizing beam splitter and a half-wave plate to control the power and polarization of the pump beam. Afterward, both beams were recombined on a 50:50 beam splitter. A 20× objective lens and numerical aperture (NA) = 0.4 focuses the probe and pump beam to a focal spot of 100 and 60 μm onto the metalens. A second identical objective mounted on a piezoelectric stage collects the light after the metalens. A band-pass filter with central frequency of 1.31 μm blocks the pump while allowing the probe to reach a near-infrared (NIR) camera and a photodiode. We acquired an image stack of 2D intensity maps along the principle optical axis with a step size of ∼1 μm by moving the collection objective with the piezo stage. First, we characterized the lens response in the absence of the pump beam. Figure 4a,b shows the 2D intensity map without pump

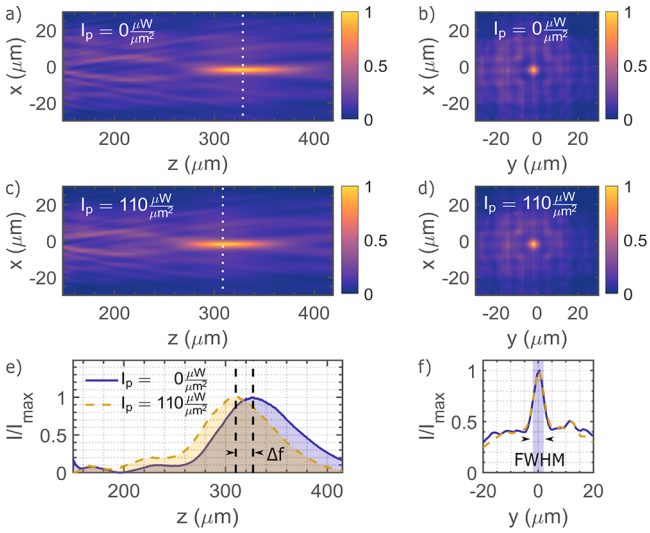

Figure 4. Optical characterization of the focal length with pump light ON and OFF. (a, c) 2D intensity maps in the xz-plane with the pump intensities $I_p = 0$ μW/μm^2 and $I_p = 110$ μW/μm^2, respectively. (b, d) 2D intensity profile of the focal spot in its respective focal plane (xy) under the pump intensities $I_p = 0$ μW/μm^2 and $I_p = 110$ μW/μm^2, respectively. (e) Axial optical intensity distribution for the two pump intensities. (f) 1D cut of the focal spot across the y-axis for the two pump intensities (blue solid line for $I_p = 0$ μW/μm^2 and yellow dashed line for $I_p = 110$ μW/μm^2. The fwhm is highlighted by the blue shaded area. All intensity profiles are normalized to the maximum probe intensity for the given pump intensity.

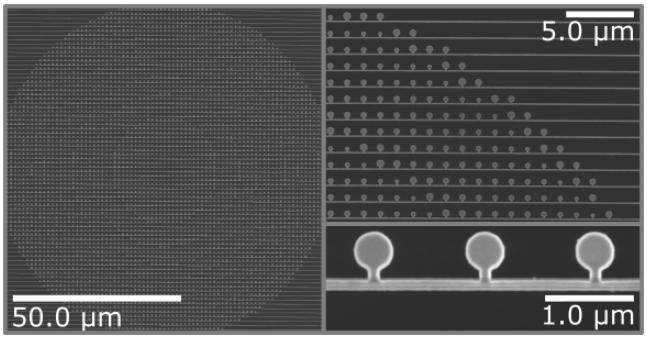

Figure 3. SEM micrographs of an optomechanically reconfigurable metalens. Fabricated metalens with diameter $D = 100$ μm and designed focal length $f = 300$ μm carved on a free-standing silicon membrane (Norcada Inc.) of thickness 200 nm.

($I_p = 0$ μW/μm^2) in the xz-plane (longitudinal) and at the focal plane (transversal), respectively. For the sake of space, we only present the axial intensity profile along the xz-plane. However, the focal length evolution is similar in the yz-plane, as the metalens confines the light in both x- and y-directions (see Figure 4b). The measured focal length is $f = 328 \pm 0.3$ μm. We also measured the transmission efficiency of the metalens in terms of the focused probe intensity as a fraction of the incident probe beam intensity to ∼47%. Subsequently, we switched on the pump beam (intensity $I_p = 110$ μW/μm^2) and observed a reduction of the focal length by $\Delta f = -20$ μm. The 2D intensity maps (longitudinal and transversal) are displayed in Figure 4c,d. For further comparison, we plot the focus profile (z-cut) and 1D focal spot profile with and without pump laser in Figure 4e,f, respectively. It is noteworthy that the focusing quality and the full width at half-maximum (fwhm)

https://doi.org/10.1021/acs.nanolett.2c04105
Nano Lett. 2023, 23, 2496−2501

value is well-preserved upon the introduction of the pump laser. Furthermore, the involved pump intensities are compatible with light-emitting diode (LED) arrays, thus eliminating the need for a bulky laser source.

Although our metalens was optimized for x-polarized pump light, we also characterized the metalens under y-polarized pump light and found a focal change $\Delta f = -6\ \mu$m for the pump intensity $I_p = 110\ \mu W/\mu m^2$ (see Figure S3 in Supporting Information). This is consistent with numerical simulations shown in Figure S4b, which reveal that, under y-polarization, the effect of the pump on the beam becomes negligible, and, in contrast to the x-polarized case, the force on the disk is along the propagation direction.

When sweeping the pump intensity I_p from 0 to 110 $\mu W/\mu m^2$, we observed a linear power dependence of the focal distance (Figure 5a). Another important parameter that

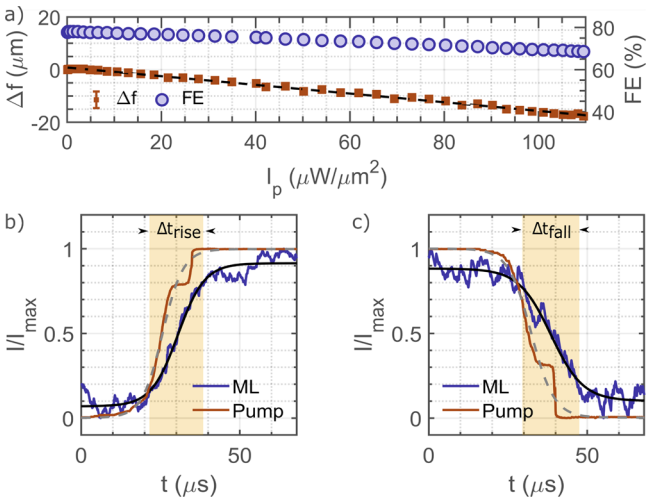

Figure 5. Focal length reconfigurability and switching dynamics of the metalens. (a) Focal length change and focusing efficiency (FE) as a function of pump intensity I_p. Red dots represent experimental data while the black solid line is a linear fit. The blue circular dots show the focusing efficiency (FE). (b) Time response (rise time) of the metalens (blue solid line) switching from f = 328 to 308 μm under modulation of the pump beam from 0 to 110 $\mu W/\mu m^2$ (red solid line). (c) Time response (fall time) of the metalens (blue solid line) switching from f = 308 to 328 μm under modulation of the pump beam from 110 to 0 $\mu W/\mu m^2$ (red solid line). In (b, c), black solid line and gray dashed lines are sigmoid fits to the metalens and pump response, respectively. The 90% to 10% rise/fall time for the metalens is higlighted by the yellow shaded area.

characterizes the performance of a metalens is the focusing efficiency (FE), defined as the fraction of the transmitted power concentrated within an aperture of radius three times the fwhm of the focal spot at the respective focal plane of the metalens.[47] We experimentally measured the FE for increasing I_p and observed a reduction from 78% (for $I_p = 0\ \mu W/\mu m^2$) to 68% (for $I_p = 110\ \mu W/\mu m^2$) as depicted in Figure 5a (blue circular dots).

Finally, we are interested in the switching dynamics of our optomechanically reconfigurable metalens. To measure its time response, we modulated the pump beam through the EOM with a square wave of frequency 0.5 Hz and amplitude 110 $\mu W/\mu m^2$. The switching on rise time (10−90%) and switching off fall time (90−10%) of the EOM is limited to 14 μs. Figure 5b,c shows the time response of both the pump (red solid curve) and the metalens (blue solid line). We fit a sigmoid function to the data (black solid line for the metalens and gray dashed line for the pump) to obtain the rise and fall times. Our measurements give a rise time Δt_{rise} = 17 μs (10% to 90%) and fall time Δt_{fall} = 18 μs (90% to 10%) for the metalens highlighted by yellow shaded area in Figure 5b,c, respectively. From these values, we rule out that thermal effects dominate in the tunability of our lens. This conclusion is corroborated by the switching time calculated by Zhang et al.[37]

In conclusion, we proposed and realized an ultrathin varifocal metalens actuated by optomechanical control, which combines significant tunability with 10 μs response time. While the system was optimized to operate in the NIR region of the spectrum, extension to the visible frequency range could be achieved through an appropriate adjustment of the meta-atoms parameters and choice of their constitutive material. We foresee that future development of optomechanical integrated reconfigurable metalenses and other metasurface-based functionalities would greatly benefit from advanced mode engineering (exploiting for instance quasi bound states in the continuum), engineering the internal residual stress and exploiting the mechanical resonance frequencies of the system.

■ ASSOCIATED CONTENT

Supporting Information

The Supporting Information is available free of charge at https://pubs.acs.org/doi/10.1021/acs.nanolett.2c04105.

Additional figures, references, and discussion (ZIP)

Numerical simulations (optical and thermal) of meta-atoms, optical force calculation, meta-atom library, optical setup for characterization of metalens, metalens performance under y-polarization pump, optical forces and actuation under y-polarized pump, meta-atom actuation as increasing beam length and characterization of structural anisotropy (PDF)

■ AUTHOR INFORMATION

Corresponding Author

Romain Quidant − *Nanophotonic Systems Laboratory, Department of Mechanical and Process Engineering, ETH Zurich, 8092 Zurich, Switzerland;* orcid.org/0000-0001-8995-8976; Email: rquidant@ethz.ch

Authors

Adeel Afridi − *ICFO Institut de Ciencies Fotoniques, 08860 Castelldefels, Barcelona, Spain; Nanophotonic Systems Laboratory, Department of Mechanical and Process Engineering, ETH Zurich, 8092 Zurich, Switzerland;* orcid.org/0000-0001-5402-7485

Jan Gieseler − *ICFO Institut de Ciencies Fotoniques, 08860 Castelldefels, Barcelona, Spain*

Nadine Meyer − *Nanophotonic Systems Laboratory, Department of Mechanical and Process Engineering, ETH Zurich, 8092 Zurich, Switzerland;* orcid.org/0000-0001-7303-0903

Complete contact information is available at: https://pubs.acs.org/10.1021/acs.nanolett.2c04105

Notes

The authors declare no competing financial interest.

https://doi.org/10.1021/acs.nanolett.2c04105
Nano Lett. 2023, 23, 2496−2501

■ ACKNOWLEDGMENTS

Adeel Afridi acknowledges financial support from the Marie Skłodowska-Curie Co-funding Programme (COFUND-DP, H2020-MSCA-COFUND-2014, GA No. 665884).

■ REFERENCES

(1) Kildishev, A. V.; Boltasseva, A.; Shalaev, V. M. Planar photonics with metasurfaces. *Science* **2013**, *339*, 1232009.
(2) Yu, N.; Capasso, F. Flat optics with designer metasurfaces. *Nat. Mater.* **2014**, *13*, 139−150.
(3) Genevet, P.; Capasso, F.; Aieta, F.; Khorasaninejad, M.; Devlin, R. Recent advances in planar optics: from plasmonic to dielectric metasurfaces. *Optica* **2017**, *4*, 139−152.
(4) Yu, N.; Genevet, P.; Kats, M. A.; Aieta, F.; Tetienne, J. P.; Capasso, F.; Gaburro, Z. Light propagation with phase discontinuities: Generalized laws of reflection and refraction. *Science* **2011**, *334*, 333−337.
(5) Khorasaninejad, M.; Capasso, F. Metalenses: Versatile multifunctional photonic components. *Science* **2017**, *358*, No. eaam8100.
(6) She, A.; Zhang, S.; Shian, S.; Clarke, D. R.; Capasso, F. Adaptive metalenses with simultaneous electrical control of focal length, astigmatism, and shift. *Sci. Adv.* **2018**, *4*, No. eaap9957.
(7) Moon, S.-W.; Kim, Y.; Yoon, G.; Rho, J. Recent progress on ultrathin metalenses for flat optics. *Iscience* **2020**, *23*, 101877.
(8) Lee, D.; Gwak, J.; Badloe, T.; Palomba, S.; Rho, J. Metasurfaces-based imaging and applications: from miniaturized optical components to functional imaging platforms. *Nanoscale Advances* **2020**, *2*, 605−625.
(9) Khorasaninejad, M.; Chen, W. T.; Devlin, R. C.; Oh, J.; Zhu, A. Y.; Capasso, F. Metalenses at visible wavelengths: Diffraction-limited focusing and subwavelength resolution imaging. *Science* **2016**, *352*, 1190−1194.
(10) Lalanne, P.; Chavel, P. Metalenses at visible wavelengths: past, present, perspectives. *Laser & Photonics Reviews* **2017**, *11*, 1600295.
(11) Tseng, M. L.; Hsiao, H.-H.; Chu, C. H.; Chen, M. K.; Sun, G.; Liu, A.-Q.; Tsai, D. P. Metalenses: advances and applications. *Advanced Optical Materials* **2018**, *6*, 1800554.
(12) Bosch, M.; Shcherbakov, M. R.; Won, K.; Lee, H. S.; Kim, Y.; Shvets, G. Electrically Actuated Varifocal Lens Based on Liquid-Crystal-Embedded Dielectric Metasurfaces. *Nano Lett.* **2021**, *21*, 3849−3856.
(13) Ee, H. S.; Agarwal, R. Tunable Metasurface and Flat Optical Zoom Lens on a Stretchable Substrate. *Nano Lett.* **2016**, *16*, 2818−2823.
(14) Kamali, S. M.; Arbabi, E.; Arbabi, A.; Horie, Y.; Faraon, A. Highly tunable elastic dielectric metasurface lenses. *Laser and Photonics Reviews* **2016**, *10*, 1002−1008.
(15) Arbabi, E.; Arbabi, A.; Kamali, S. M.; Horie, Y.; Faraji-Dana, M.; Faraon, A. MEMS-tunable dielectric metasurface lens. *Nat. Commun.* **2018**, *9*, 1−9.
(16) Shen, Z.; Zhou, S.; Li, X.; Ge, S.; Chen, P.; Hu, W.; Lu, Y. Liquid crystal integrated metalens with tunable chromatic aberration. *Advanced Photonics* **2020**, *2*, 036002.
(17) Fan, C.-Y.; Chuang, T.-J.; Wu, K.-H.; Su, G.-D. J. Electrically modulated varifocal metalens combined with twisted nematic liquid crystals. *Opt. Express* **2020**, *28*, 10609.
(18) Badloe, T.; Kim, I.; Kim, Y.; Kim, J.; Rho, J. Electrically tunable bifocal metalens with diffraction-limited focusing and imaging at visible wavelengths. *Advanced Science* **2021**, *8*, 2102646.
(19) Archetti, A.; Lin, R.-J.; Restori, N.; Kiani, F.; Tsoulos, T. V.; Tagliabue, G. Thermally reconfigurable metalens. *Nanophotonics* **2022**, *11* (17), 3969−3980.
(20) Afridi, A.; Canet-Ferrer, J.; Philippet, L.; Osmond, J.; Berto, P.; Quidant, R. Electrically Driven Varifocal Silicon Metalens. *ACS Photonics* **2018**, *5*, 4497−4503.
(21) Yao, B.; Zang, X.; Zhu, Y.; Yu, D.; Xie, J.; Chen, L.; Han, S.; Zhu, Y.; Zhuang, S. Spin-decoupled metalens with intensity-tunable multiple focal points. *Photonics Research* **2021**, *9*, 1019.
(22) Wang, W.; Kang, C.; Liu, X.; Qu, S. Spin-selected and spin-independent dielectric metalenses. *Journal of Optics* **2018**, *20*, 095102.
(23) Groever, B.; Rubin, N. A.; Mueller, J.; Devlin, R. C.; Capasso, F. High-efficiency chiral meta-lens. *Sci. Rep.* **2018**, *8*, 1−6.
(24) Fu, R.; Li, Z.; Zheng, G.; Chen, M.; Yang, Y.; Tao, J.; Wu, L.; Deng, Q. Reconfigurable step-zoom metalens without optical and mechanical compensations. *Opt. Express* **2019**, *27*, 12221.
(25) Yu, L.; Fan, Y.; Wang, Y.; Zhang, C.; Yang, W.; Song, Q.; Xiao, S. Spin angular momentum controlled multifunctional all-dielectric metasurface doublet. *Laser & Photonics Reviews* **2020**, *14*, 1900324.
(26) Shalaginov, M. Y.; An, S.; Zhang, Y.; Yang, F.; Su, P.; Liberman, V.; Chou, J. B.; Roberts, C. M.; Kang, M.; Rios, C.; et al. Reconfigurable all-dielectric metalens with diffraction-limited performance. *Nat. Commun.* **2021**, *12*, 1−8.
(27) Mikheeva, E.; Kyrou, C.; Bentata, F.; Khadir, S.; Cueff, S.; Genevet, P. Space and Time Modulations of Light with Metasurfaces: Recent Progress and Future Prospects. *ACS Photonics* **2022**, *9*, 1458−1482.
(28) Yang, J.; Gurung, S.; Bej, S.; Ni, P.; Howard Lee, H. W. Active optical metasurfaces: comprehensive review on physics, mechanisms, and prospective applications. *Rep. Prog. Phys.* **2022**, *85*, 036101.
(29) Gartner, C.; Moura, J. P.; Haaxman, W.; Norte, R. A.; Groblacher, S. Integrated optomechanical arrays of two high reflectivity SiN membranes. *Nano Lett.* **2018**, *18*, 7171−7175.
(30) Moura, J. P.; Norte, R. A.; Guo, J.; Schäfermeier, C.; Gröblacher, S. Centimeter-scale suspended photonic crystal mirrors. *Opt. Express* **2018**, *26*, 1895−1909.
(31) Burgwal, R.; Pino, J. d.; Verhagen, E. Comparing nonlinear optomechanical coupling in membrane-in-the-middle and single-cavity systems. *New J. Phys.* **2020**, *22*, 113006.
(32) La Gala, G.; P Mathew, J.; Neveu, P.; Verhagen, E. Nanomechanical design strategy for single-mode optomechanical measurement. *J. Phys. D: Appl. Phys.* **2022**, *55*, 225101.
(33) Norte, R. A.; Moura, J. P.; Gröblacher, S. Mechanical resonators for quantum optomechanics experiments at room temperature. *Physical review letters* **2016**, *116*, 147202.
(34) Zhu, H.; Yi, F.; Cubukcu, E. Plasmonic metamaterial absorber for broadband manipulation of mechanical resonances. *Nat. Photonics* **2016**, *10*, 709−714.
(35) Zanotto, S.; Tredicucci, A.; Navarro-Urrios, D.; Cecchini, M.; Biasiol, G.; Mencarelli, D.; Pierantoni, L.; Pitanti, A. Optomechanics of chiral dielectric metasurfaces. *Advanced Optical Materials* **2020**, *8*, 1901507.
(36) Zheludev, N. I.; Plum, E. Reconfigurable nanomechanical photonic metamaterials. *Nat. Nanotechnol.* **2016**, *11*, 16−22.
(37) Zhang, J.; MacDonald, K. F.; Zheludev, N. I. Nonlinear dielectric optomechanical metamaterials. *Light: Science & Applications* **2013**, *2*, e96−e96.
(38) Karvounis, A.; Ou, J. Y.; Wu, W.; Macdonald, K. F.; Zheludev, N. I. Nano-optomechanical nonlinear dielectric metamaterials. *Appl. Phys. Lett.* **2015**, *107*, 191110.
(39) Ou, J.-Y.; Plum, E.; Zheludev, N. I. Optical addressing of nanomechanical metamaterials with subwavelength resolution. *Appl. Phys. Lett.* **2018**, *113*, 081104.
(40) Ajia, I. A.; Ou, J. Y.; Dinsdale, N. J.; Singh, H. J.; Chen-Sverre, T.; Liu, T.; Zheludev, N. I.; Muskens, O. L. Gigahertz Nano-Optomechanical Resonances in a Dielectric SiC-Membrane Metasurface Array. *Nano Lett.* **2021**, *21*, 4563−4569.
(41) Sang, Y.; Xu, J.; Liu, K.; Chen, W.; Xiao, Y.; Zhu, Z.; Liu, N.; Zhang, J. Spatial Nonreciprocal Transmission and Optical Bistability Based on Millimeter-Scale Suspended Metasurface. *Advanced Optical Materials* **2022**, *10*, 2201523.
(42) Decker, M.; Staude, I.; Falkner, M.; Dominguez, J.; Neshev, D. N.; Brener, I.; Pertsch, T.; Kivshar, Y. S. High-efficiency dielectric Huygens' surfaces. *Advanced Optical Materials* **2015**, *3*, 813−820.
(43) Yu, Y. F.; Zhu, A. Y.; Paniagua-Domínguez, R.; Fu, Y. H.; Luk'yanchuk, B.; Kuznetsov, A. I. High-transmission dielectric metasurface with 2π phase control at visible wavelengths. *Laser & Photonics Reviews* **2015**, *9*, 412−418.

https://doi.org/10.1021/acs.nanolett.2c04105
Nano Lett. 2023, 23, 2496−2501

(44) Middelmann, T.; Walkov, A.; Bartl, G.; Schödel, R. Thermal expansion coefficient of single-crystal silicon from 7 to 293 K. *Phys. Rev. B* **2015**, *92*, 174113.
(45) Watanabe, H.; Yamada, N.; Okaji, M. Development of a laser interferometric dilatometer for measurements of thermal expansion of solids in the temperature range 300 to 1300 K. *Int. J. Thermophys.* **2002**, *23*, 543−554.
(46) Watanabe, H.; Yamada, N.; Okaji, M. Linear thermal expansion coefficient of silicon from 293 to 1000 K. *Int. J. Thermophys.* **2004**, *25*, 221−236.
(47) Lin, H.; Xu, Z.-Q.; Cao, G.; Zhang, Y.; Zhou, J.; Wang, Z.; Wan, Z.; Liu, Z.; Loh, K. P.; Qiu, C.-W.; et al. Diffraction-limited imaging with monolayer 2D material-based ultrathin flat lenses. *Light Sci. Appl.* **2020**, *9*, 1−11.

https://doi.org/10.1021/acs.nanolett.2c04105
Nano Lett. 2023, 23, 2496−2501